Desalination and Water Treatment
www.deswater.com
doi: 10.1080/19443994.2016.1193767

57 (2016) 28794–28805
December

Taylor & Francis
Taylor & Francis Group

Equilibrium and kinetics studies of adsorption phosphate on raw and novel lithium silica fume based adsorbent

Yuguo Lai, Wenju Jiang, Zhishan Yang, Xianpeng Hao, Ruzhen Xie*

College of Architecture and Environment, Sichuan University, Chengdu 610065, China, Tel. +86 28 8540 3016; Fax: +86 28 8540 5613; emails: laiyuguo920303@163.com (Y. Lai), wenjujiang@scu.edu.cn (W. Jiang), yangzs@scu.edu.cn (Z. Yang), 649337523@qq.com (X. Hao), xieruzhen@scu.edu.cn (R. Xie)

Received 16 December 2015; Accepted 19 May 2016

ABSTRACT

In this study, the adsorption of phosphate from aqueous solution by lithium silica fume (LSF) with or without iron oxides modification was investigated. Iron oxides modification was achieved by *in situ* generation of iron oxides on LSF by applying three different kinds of ferric solution ($FeCl_3{\cdot}6H_2O$, $Fe(NO_3)_3{\cdot}9H_2O$, and $Fe_2(SO_4)_3$) with Na_2CO_3 addition. Batch adsorption studies were carried out for better understanding of their adsorption behaviors towards phosphate. Among three iron oxide modified adsorbents, $FeCl_3$-modified LSF ($FeCl_3$/LSF) exhibited highest S_{BET}, and best adsorptive capability towards phosphate. The adsorption kinetics data of phosphate adsorption onto $FeCl_3$/LSF fitted well with Langmuir model and Freundlich model. The maximum phosphate adsorption capacity onto $FeCl_3$/LSF is 13.39 mg g^{-1} at 25°C, almost three times higher than that of LSF. The X-ray diffraction pattern showed new species of $Fe(PO_3)_3$ that was formed on $FeCl_3$/LSF after adsorbing onto phosphate, which indicated chemisorption was involved in phosphate adsorption; this phenomenon is in accordance with SEM-EDS, FTIR, and X-ray photoelectron spectroscopy analysis. The coexistence of Cl^-, NO_3^-, SO_4^{2-} slightly affected phosphate removal, while coexistence of CO_3^{2-} greatly reduced the adsorption of phosphate. The relatively low cost and high capabilities of $FeCl_3$/LSF make it a potentially attractive adsorbent for removing phosphate from aqueous solution.

Keywords: Iron oxide modified lithium silica fume; Phosphate removal; Adsorption behavior; Isotherms; Kinetics

1. Introduction

Phosphorous is an essential element in biological organisms not only for plants and animals, but also for bacteria and fungi [1]. However, phosphorus is a non-renewable resource, and would be depleted within 50–100 years [2,3]. The accumulation of phosphorous in stagnant water bodies from phosphate containing industrial wastewater and domestic wastewater can cause eutrophication [4,5]. Eutrophication process poses a great threat to the balance of aquatic ecosystem by the consumption of dissolved oxygen in water. Therefore, it is necessary to remove excess phosphate before discharging wastewater into water bodies.

Various methods such as chemical precipitation, biodegradation and adsorption have been applied for

*Corresponding author.

1944-3994/1944-3986 © 2016 Balaban Desalination Publications. All rights reserved.

phosphate removal [4,6–8]. However, the efficiency of biological process is limited by microbiological conditions and composition of wastewater. What's more, excess sludge produced by the biological processes is another problem. Chemical precipitation is a widely used method to remove phosphate with high efficiency. But, it has been hindered by its high cost and chemical consumption [7,9]. Adsorption is an alternative method to remove phosphate for its high removal efficiency, easy operation, and adaptive to different water conditions [10–12]. In recent years, various industrial wastes or by-products have been applied as adsorbents to remove phosphate from wastewater, including coal fly ash [6,13,14], phosphate mine slimes [15], red mud [16–18], ferric sludge [19], dewatered alum sludge [20], etc. Although these kinds of adsorbents are cost-effective, their uptake capacities towards phosphate are low, and need to be modified [3,21,22].

Lithium silica fume (LSF) is a waste product derived from the process of lithium salt production. It is a crystalline and porous material mainly consisting of SiO_2 and it has the potential to be used as adsorbent. Researchers found that immobilizing enzyme such as laccase, apocarbonic anhydrase, and methylobacterium extorquens, would largely improve the adsorption capacity of silica fume. The modified silica fume exhibited better removal capacity towards metal ions and dyes [23–28]. Besides, rare earth metals such as lanthanum, were widely applied to modify adsorbents' surface. Huang et al. [21] prepared lanthanum-doped ordered mesoporous hollow silica spheres adsorbent. Reitzel et al. [29] investigated lanthanum-modified bentonite clay. Shin et al. [30] applied lanthanum to modify lignocellulosic sorbents. Since lanthanum could bind the phosphorus and form precipitates, lanthanum-modified adsorbents exhibit high phosphate uptake capacity. However, the relative high cost and secondary pollution caused by rare earth metal release hindered their extensive application [31–33]. Iron oxide is a kind of adsorbent with large surface area and various binding sites on its surface [34–36]. It has been extensively applied to remove contaminants from aqueous solution, such as phosphate, cadmium, and arsenite [37–39]. Besides, they can be impregnated onto various materials such as activated carbon, diatomite, and sand to improve their adsorption capacities [39–41].

The aim of this study was to develop an efficient adsorbent from industrial waste—LSF as raw material to remove phosphate from wastewater. Iron oxides instead of expensive chemical agent were employed as additives. LSF with or without iron oxide modification were investigated for their adsorption capacity towards phosphate in aqueous solution. To understand the adsorptive behavior of phosphate on these adsorbents, the effect of adsorbent dosage, initial solution pH, and coexisting ions on the phosphate adsorption were investigated. Adsorption kinetics, adsorption isotherms, and thermodynamic were also studied for further understanding the adsorption mechanism. The results would provide new insights on the development of high performance adsorbent with low cost for phosphate removal.

2. Materials and methods

2.1. Materials

LSF used in this study was obtained from a Regenerated Resources Recycling Co., Ltd. of Sichuan province, China. It was used as raw material to prepare adsorbents. LSF mainly consists of (wt.%): SiO_2, 60.0; CaO, 4.28; Al_2O_3, 18.33; SO_3, 6.08; MgO, 0.42; K_2O, 0.73; Fe_2O_3, 0.56; Li_2O, 0.43; Na_2O, 0.36; H_2O, 2.0; Heat loss, 6.81. Chemicals and reagents such as $FeCl_3{\cdot}6H_2O$, $Fe(NO_3)_3{\cdot}9H_2O$, $Fe_2(SO_4)_3$, KH_2PO_4, NaOH were of analytical reagent grade.

2.2. Preparation of adsorbents

For adsorbent preparation, 100 mL 0.5 mol L^{-1} Na_2CO_3 solution was dropwise added into 150 mL 0.5 mol L^{-1} ferric solution ($FeCl_3{\cdot}6H_2O$ solution, $Fe(NO_3)_3{\cdot}9H_2O$ solution, $Fe_2(SO_4)_3$ solution) with or without LSF (V_{liquid}/m_{solid} = 5:1) addition, the solution was continuously stirred for 2 h. After that, the mixed solution was kept in thermostatic chamber at 60°C for 48 h. The solids were collected after centrifugation, and washed with distilled water to neutral pH and dried at 105°C for 8 h. Finally the products were ground and sieved to pass through a 200-mesh screen. For iron oxides, granules produced by $FeCl_3{\cdot}6H_2O$, $Fe(NO_3)_3{\cdot}9H_2O$, and $Fe_2(SO_4)_3$ without LSF addition was named as "$Fe_2O_3/FeCl_3$," "$Fe_2O_3/Fe(NO_3)_3$," and "$Fe_2O_3/Fe_2(SO_4)_3$," respectively. For those modified with LSF, addition was designated as "$FeCl_3$/LSF," "$Fe(NO_3)_3$/LSF," and "$Fe_2(SO_4)_3$/LSF," respectively.

2.3. Characterization of adsorbents

BET surface area were measured by N_2 adsorption–desorption technique with a surface area analyzer (ASAP 2046, Micromeritics, USA) at 77 K. Scanning electron microscopy (JSM-7500F, JEOL) with an Energy Dispersion X-ray (X-Max 51-XM X0019, Oxford Instruments) was employed to observe the morphology and surface element composition on the adsorbents.

The crystal structure of adsorbents before and after adsorption were measured by a X-ray diffraction (XRD) with an X-Pert PRO MP D diffractometer (Panalytical, NL) using Cu Kα radiation at 30 kV and 20 mA over 2θ range of 10°–80°. IR analysis of adsorbents were performed to detect vibration frequency changes before and after adsorbing phosphate using Fourier transform infrared spectroscopy (FTIR 6700 NEXUS Nicolet, USA). X-ray photoelectron spectroscopy (XPS) was applied to determine the surface chemical composition and functional groups, using a XSAM-800 spectrometer (KRATOS, UK) with Al (1,486.6 eV) under ultra-high vacuum (UHV) at 12 kV and 15 mA. Iron leaching study was carried out using an atomic absorption spectrometer (SpectrAA 220FS). The pH point of zero charge (pHzpc) was measured to investigate the total surface charge of the adsorbents using the method described by Su et al. [42].

2.4. Phosphate adsorption experiments

Synthetic phosphate stock solution of 1,000 mg L^{-1} was prepared by dissolving a certain amount of analytical grade anhydrous potassium dihydrogen phosphate (KH_2PO_4) in distilled water. Then the stock solution was diluted with distilled water for desired concentrations. The adsorbent dosage study was carried out by adding different amount of adsorbents (0.05–1.0 g) in a series of 250 mL conical flask containing 100 mL and 10 mg L^{-1} phosphate solution. About 0.1 mol L^{-1} HCl or 0.1 mol L^{-1} NaOH was used to adjust initial solution to pH 7. The suspensions were shaken in a thermostatic chamber at 25 ± 1°C at 180 rpm. After 180 min, the suspension was filtered through 0.45 μm membrane filters. The filtrate was determined for phosphate concentration, using the molybdenum-blue ascorbic-acid method [3,43]. The effect of initial solution pH was studied by adjusting the pH of the solution from 1 to 12 with adsorbents' dosage of 1.5 g L^{-1}. In kinetics study, 1.2 g samples were added into 800 mL 10 mg L^{-1} phosphate solution, and then stirred at 25 ± 1°C at 180 rpm with initial solution pH of 7. After 6 h, 20 mL of solution sample was taken at certain time intervals to determine the phosphate concentration. Adsorption isotherms of phosphate were performed with 1.5 g L^{-1} of adsorbent under three different temperatures (25, 35, and 45°C) with initial phosphate concentrations of 5–100 mg L^{-1}. The equilibrium adsorption capacity was calculated as follows:

$$Q = \frac{(C_0 - C_e)V}{m} \quad (1)$$

where C_0 is the initial phosphate concentration, C_e is the equilibrium phosphate concentration, V is the sample volume in litre, and m is the dry weight of adsorbent in grams.

2.5. Influence of coexisting anions

To evaluate the influence of coexisting anions on the performance of the adsorbents, 0.01 mol L^{-1} Cl^-, NO_3^-, SO_4^{2-}, and CO_3^{2-} was added, respectively, into phosphate solutions (10 mg L^{-1}, 100 mL) containing 0.15 g adsorbent. After shaking for 3 h at 25°C, residue phosphate concentration was evaluated.

2.6. Regeneration of adsorbent

The regeneration procedures containing adsorption process and desorption process were repeated for three cycles. For adsorption process, adsorbent was reacted for 3 h in 1,000 mL 10 mg L^{-1} phosphate solution to reach equilibrium. After that, the adsorbent was collected by filtration and dried for 8 h at 105°C. The regeneration process was conducted by reacting 1 g dried adsorbent sample in 100 mL, 3 mol L^{-1} NaOH for 5 h at 25 ± 1°C. The desorption suspension solution was filtered and the amount of desorbed phosphate was determined. Regenerated adsorbent was washed with distilled water until the filtrate to neutral pH before the next cycle of adsorption and desorption.

3. Results and discussion

3.1. Characterization of adsorbents

3.1.1. BET analysis

The BET analysis is presented in Table 1. As can be seen from Table 1, the average pore size of LSF, $FeCl_3$/LSF, $Fe(NO_3)_3$/LSF, and $Fe_2(SO_4)_3$/LSF were between 2 and 10 nm, all these adsorbents possess mesopores. BET surface area of $FeCl_3$/LSF, $Fe(NO_3)_3$/LSF, and $Fe_2(SO_4)_3$/LSF were 68.9, 65.6, and 62.3 m^2 g^{-1}, respectively, which is almost four times higher than that of LSF(14.4 m^2 g^{-1}). Iron oxides modified LSF showed higher BET surface area than unmodified LSF, thus resulting in higher phosphate adsorption capacity. Among these adsorbents, $FeCl_3$/LSF exhibited the best porous characteristic, with highest BET surface area of 68.9 m^2 g^{-1} and largest pore volume of 0.049 cm^3 g^{-1}. This result indicated that $FeCl_3 \cdot 6H_2O$-modified LSF might be more favorable for phosphate adsorption.

Table 1
BET analysis results of LSF with or without iron oxides modification

Samples	BET Surface ($m^2\ g^{-1}$)	Pore volume ($cm^3\ g^{-1}$)	Average pore diameter (nm)
LSF	14.4	0.032	9.03
$FeCl_3$/LSF	68.9	0.049	3.18
$Fe(NO_3)_3$/LSF	65.6	0.046	3.37
$Fe_2(SO_4)_3$/LSF	62.3	0.040	6.17

3.1.2. SEM–EDS analysis

The SEM images of $FeCl_3$/LSF before and after phosphate adsorption are shown in Fig. 1. From the micrograph in Fig. 1(a) and (b), we can see porous structures in $FeCl_3$/LSF, and similar morphology was observed in $FeCl_3$/LSF before and after adsorbing phosphate. From EDS results, chloride peak can be observed in the spectra of $FeCl_3$/LSF before adsorption (Fig. 2(b)), which could be attributable to the residue of $FeCl_3$. After adsorbing phosphate, the chloride peak disappeared. The disappearance of chloride peak may be due to ligand exchange between chloride present on the surface of $FeCl_3$/LSF and phosphate ions in the aqueous solution [15].

3.1.3. XRD analysis

Fig. 3 showed the XRD patterns of $FeCl_3$/LSF before and after phosphate adsorption. The phases of $LiAlSi_2O_6$, SiO_2, and Fe + 3O(OH) were identified on $FeCl_3$/LSF, which are main crystal structures of $FeCl_3$/LSF. After adsorbing phosphate, a significant

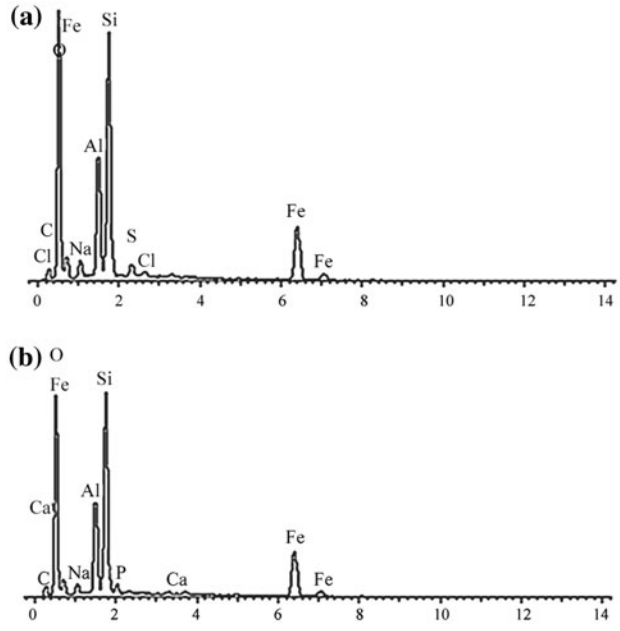

Fig. 2. EDS images of $FeCl_3$/LSF before (a) and after (b) phosphate adsorption.

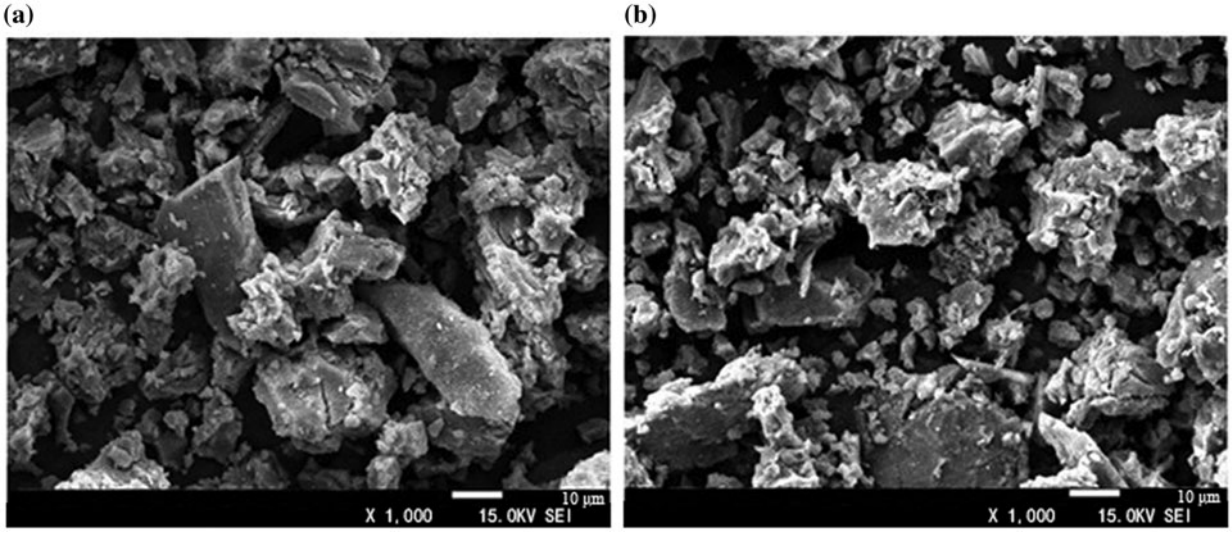

Fig. 1. SEM images of $FeCl_3$/LSF before (a) and after (b) phosphate adsorption.

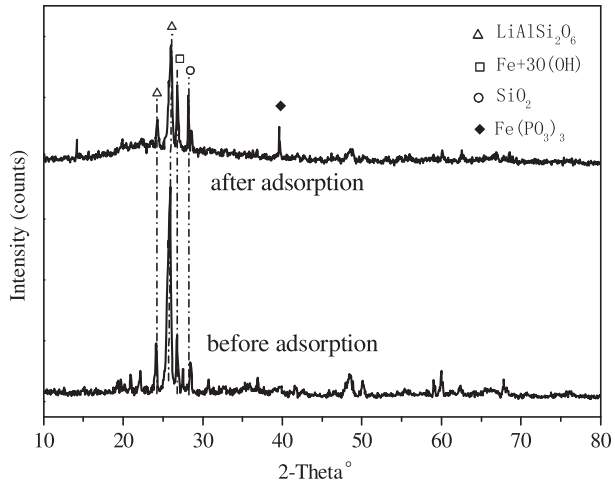

Fig. 3. XRD pattern of $FeCl_3$/LSF before and after phosphate adsorption.

characteristic peak of $Fe(PO_3)_3$ at $2\theta = 4.204^\circ$ (JCPDs13-0263) and 39.618° (JCPDs19-0638) could be observed on $FeCl_3$/LSF. The generation of chemical precipitation of $Fe(PO_3)_3$ on the surface of $FeCl_3$/LSF indicated chemisorption process was involved.

3.1.4. FTIR analysis

The FTIR spectra of $FeCl_3$/LSF before and after adsorption could be found in Fig. 4. As shown in Fig. 4, the spectrum before and after adsorption were similar, except for a slight difference in the band around 1,020 cm^{-1}, which could be attributable to the structural diagnosis of metal phosphate complexes in aqueous solution after adsorbing phosphate [20].

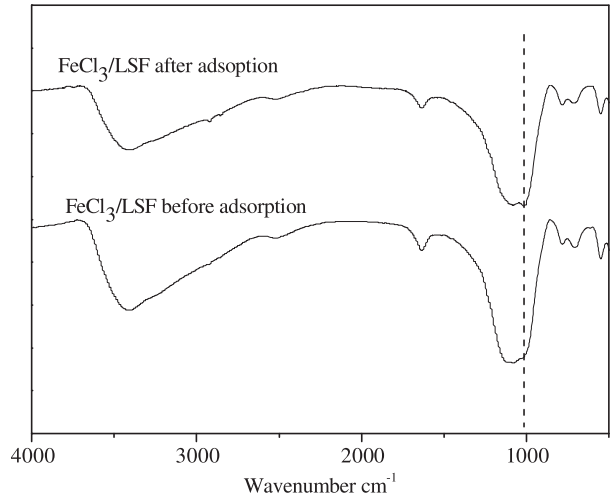

Fig. 4. The FTIR spectra of $FeCl_3$/LSF before and after phosphate adsorption.

3.1.5. XPS analysis

XPS was used to investigate the composition and chemical state of $FeCl_3$/LSF before and after adsorption. Fig. 5(a) presents the full-range survey spectra of $FeCl_3$/LSF and P-loaded $FeCl_3$/LSF. The P2p spectra on full-range survey of P-loaded $FeCl_3$/LSF indicated the adsorption of phosphate onto $FeCl_3$/LSF.

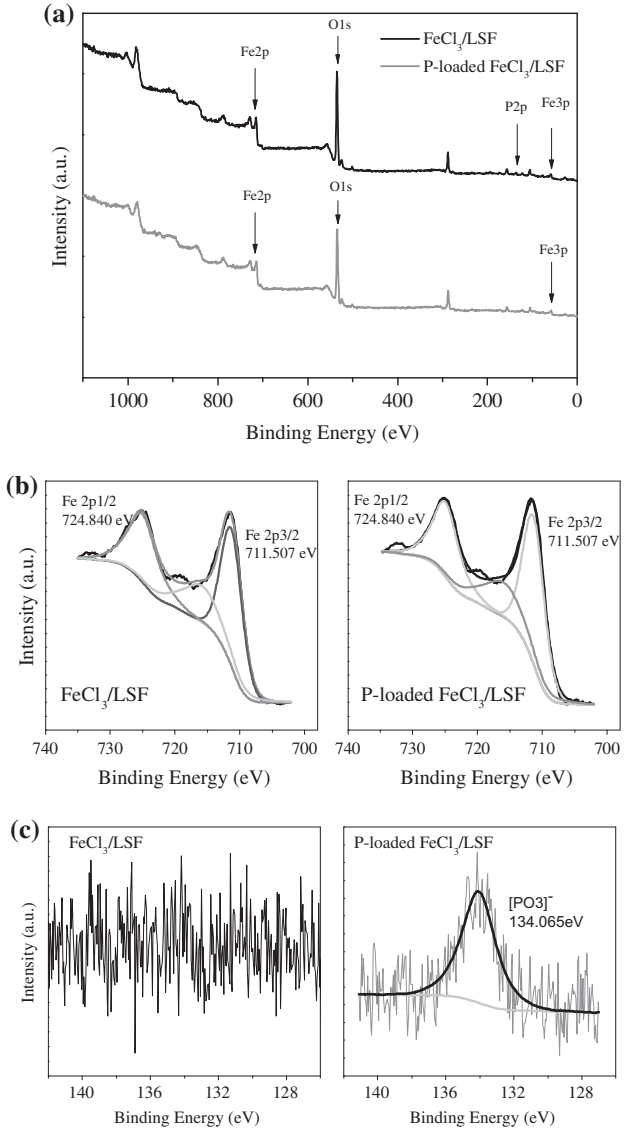

Fig. 5. The XPS spectra of $FeCl_3$/LSF before and after phosphate adsorption (a) full-range survey spectra of $FeCl_3$/LSF and P-loaded $FeCl_3$/LSF; (b) Fe2p narrow spectra in $FeCl_3$/LSF and P-loaded $FeCl_3$/LSF; (c) P2p narrow spectra in $FeCl_3$/LSF and P-loaded $FeCl_3$/LSF).

Detailed XPS surveys on the Fe2p and P2p of $FeCl_3$/LSF before and after adsorption are shown in Fig. 5(b) and (c). The binding energies at 711.507 and 724.840 eV were assigned to $Fe2p_{3/2}$ and $Fe2p_{1/2}$, and the separation of the $Fe2p_{3/2}$ and $Fe2p_{1/2}$ spin-orbit levels was 13.3 eV which was attributed to Fe(III) ions [43]. From Fig. 5(c), a peak at 134.065 eV can be found in P2p deconvoluted spectra after phosphate adsorption, which could be attributable to metaphosphates $[PO_3]^-$ binding. The XPS results confirm the XRD and FTIR analysis.

3.2. Effect of dosage

The effect of dosage on phosphate adsorption by LSF before and after modification is shown in Fig. 6. It can be observed that phosphate removal efficiency increased with the increment in adsorbent dosage, this could be due to larger surface area and the increment in available adsorptive sites with increasing adsorbent dosage. It can also be observed that the removal of phosphate became nearly constant with adsorbent dosage higher than 1.5 g L^{-1}. This could be attributable to the achievement of saturation state beyond a certain dosage during adsorption process [44]. Therefore, the optimum dosage of 1.5 g L^{-1} was fixed for the subsequent experiments. It's obvious that the adsorption capacity of iron oxides modified LSF were much higher than that of unmodified LSF.

3.3. Influence of pH value

The influence of pH value on the removal of phosphate by LSF before and after modification were investigated by carrying out the experiments at variable pH of 1, 3, 5, 7, 10, and 12, with phosphate concentration of 10 mg L^{-1}. The results are shown in Fig. 7. As can be seen from Fig. 7, phosphate adsorption by LSF before and after modification, were both profoundly affected by initial solution pH. It was observed that the maximum phosphate adsorption capacity of $Fe(NO_3)_3$/LSF, $FeCl_3$/LSF, and $Fe_2(SO_4)_3$/LSF occurred at pH 5, with adsorption amount of 6.26, 6.29, and 5.49 mg g^{-1}, respectively. While the maximum phosphate adsorption capacity achieved by LSF, was 1.25 mg g^{-1} at pH 7 as we know, the effect of pH on phosphate adsorption is governed not only by phosphate speciation in solution, but also by pH_{zpc} of adsorbent and the affinity of phosphate ions towards the adsorbent. Phosphate dissociation equilibrium in aqueous solution are pH-related and can be described as Eqs. (2)–(4) [45]. The pH_{zpc} of LSF, $Fe(NO_3)_3$/LSF, $FeCl_3$/LSF, and $Fe_2(SO_4)_3$/LSF was found to be 7.19, 4.0, 5.45, and 5.55, respectively. As can be seen from Fig. 7, all the adsorbents exhibited better adsorption capacity in the pH range of 3–7. $FeCl_3$/LSF exhibited highest phosphate uptake capability, and the optimum removal efficiency of $FeCl_3$/LSF was observed at pH around 5. Since the pH_{zpc} of $FeCl_3$/LSF is 5.45, with solution pH value between 3 and 5, the surface of $FeCl_3$/LSF was positively charged, which favored the electrostatic attraction to phosphate species $H_2PO_4^-$, which is the main species in the solution within this pH range. On the contrary, at pH higher than 5, $FeCl_3$/LSF surface was negatively charged, and negatively charged surface is more favorable for adsorbing cationic ions, thus the phosphate removal efficiency

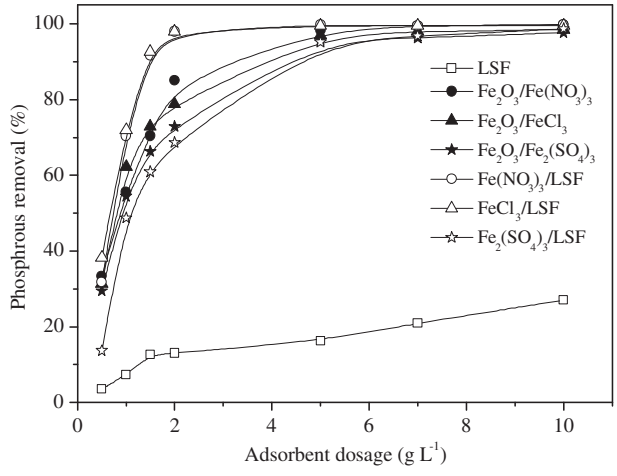

Fig. 6. Influence of adsorbent dosage on the adsorption of phosphate by iron oxides graunles and LSF before and after modification (initial phosphate concentration = 10 mg L^{-1}, contact time = 3 h, initial solution pH 7).

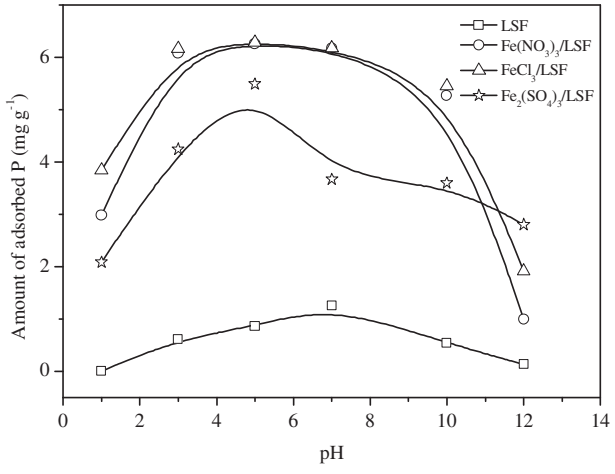

Fig. 7. Adsorption of phosphate by LSF before and after modification under different initial pH (initial phosphate concentration = 10 mg/L, dosage = 1.5 g L^{-1}, contact time = 3 h).

decreased. When pH value was further increased to more than 9, there were more OH^- ions that could compete with phosphate for adsorption sites, resulting in further decrement in phosphate removal.

$$H_3PO_4 \longleftrightarrow H^+ + H_2PO_4^- \quad pK_1 = 2.1 \tag{2}$$

$$H_2PO_4^- \longleftrightarrow H^+ + HPO_4^{2-} \quad pK_2 = 7.2 \tag{3}$$

$$HPO_4^{2-} \longleftrightarrow H^+ + PO_4^{3-} \quad pK_3 = 12.2 \tag{4}$$

At pH value lower than 3.0, the predominant species of phosphate is H_3PO_4; as protonated substance, H_3PO_4 can hardly attach to the sites of the adsorbent [46]. Besides, iron oxide would undergo dissolution at pH lower than 3 [47]. The optimum pH was also found to be 5 in the adsorption of phosphate by ferric sludge [19]. From Fig. 7, we can also see that, at pH 7, the amount of phosphate adsorption onto $FeCl_3$/LSF and $Fe(NO_3)_3$/LSF were slightly less than the amount being adsorbed at pH 5, and the maximum adsorption capacity of LSF occurred at around pH 7. Considering the effluent pH from sewage treatment plant commonly ranging from 6 to 9, we choose neutral pH of 7 for subsequent experiments.

3.4. Kinetic studies

As shown in Fig. 8, the adsorption (up to 6 h) of phosphate to LSF before and after modification was time-dependent. The removal of phosphate was initially rapid and achieved almost 80% removal efficiency within 1 h. After that, the rate of phosphate uptake decreased with extended reaction time, and reached equilibrium after 3 h.

Kinetic studies are extremely useful for understanding the mechanisms of the phosphate adsorption. In this study, the kinetic data were fitted to pseudo-first-order (Eq. (5)) and pseudo-second-order (Eq. (6)) model, which are frequently used to elaborate the mechanisms of adsorption process [15,45]:

$$\ln(Q_e - Q_t) = \ln Q_{e1} - k_1 t \tag{5}$$

$$\frac{t}{Q_t} = \frac{1}{k_2 Q_{e2}^2} + \frac{1}{Q_{e2}} t \tag{6}$$

Eqs. (5) and (6) are the linear forms of pseudo-first-order and pseudo-second-order. Where Q_e and Q_t are the amounts of phosphate adsorbed (mg g^{-1}) at any time and at equilibrium time, respectively. Q_{e1} and Q_{e2} are calculated adsorbed phosphate capacities from pseudo-first-order and pseudo-second-order, respectively. k_1 and k_2 are rate constants for pseudo-first-order and pseudo-second-order, respectively.

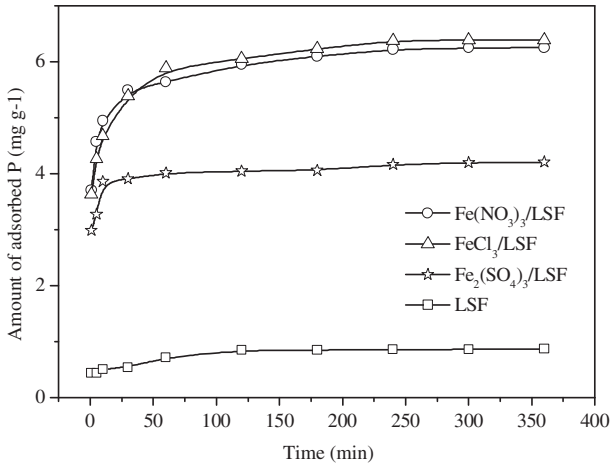

Fig. 8. Adsorption of phosphate by LSF before and after modification under different reaction time (initial phosphate concentration = 10 mg L^{-1}, dosage = 1.5 g L^{-1}, initial solution pH 7).

The kinetic results of the removal of phosphate by four adsorbents are shown in Table 2. Based on the comparison of the R^2 values in Table 2, the pseudo-second-order model was found to fit best to the experimental data. A similar result was reported by Song et al. [19] when studying the adsorption of phosphate on iron-based adsorbents. The pseudo-second-order rate (k_2) constants for LSF was higher than that of iron oxides modified LSF, suggesting higher adsorption rate and larger amount of phosphate adsorbed per unit mass of the adsorbent on iron oxides modified LSF [48]. The increment adsorption capacity achieved by iron oxides modified LSF may possibly be ascribed to the formation of $Fe(PO_3)_3$ compounds and a higher BET surface area.

From the results of dosage, pH and kinetic studies, $FeCl_3$/LSF was found to exhibit the highest adsorption capacity compared with the other two types of iron oxides modified LSF.

3.5. Adsorption isotherms

The experimental data for adsorption isotherms of phosphate adsorption on $FeCl_3$/LSF and LSF were fitted to the Langmuir and Freundlich models. The linear forms of these two models are described in Eqs. (7) and (8) [37,45]:

Table 2
Kinetic parameters of the pseudo-first-order and pseudo-second-order models for phosphate adsorption on $FeCl_3$/LSF

	Adsorbent			
	$FeCl_3$/LSF	$Fe(NO_3)_3$/LSF	$Fe_2(SO_4)_3$/LSF	LSF
Experimental Q_e (mg g^{-1})	6.39	6.25	4.21	0.87
Irreversible first-order				
k_1 (min^{-1})	0.018	0.021	0.013	0.015
Calculated Q_{e1} (mg g^{-1})	2.27	2.24	0.71	0.37
R^2	0.912	0.926	0.878	0.924
Pseudo-second-order				
k_2 (g mg^{-1} min^{-1})	0.035	0.042	0.102	0.129
Calculated Q_{e2} (mg g^{-1})	6.46	6.31	4.22	0.89
R^2	0.999	0.999	0.999	0.999

$$\frac{C_e}{Q_e} = \frac{1}{K_L Q_m} + \frac{1}{Q_m} C_e \quad (7)$$

$$\ln Q_e = \ln K_F + \frac{1}{n}(\ln C_e) \quad (8)$$

where Q_e (mg g^{-1}) and C_e (mg L^{-1}) are the equilibrium adsorbate concentration in the aqueous and solid phases. Q_m is the maximum adsorption capacity (mg g^{-1}). K_L and K_F are the Langmuir and Freundlich equilibrium constant, n is the Freundlich isotherm curvature.

The adsorption isotherms results are shown in Figs. 9–10 and Table 3. As can be seen from Table 3, both Freundlich model and Langmuir model fitted better to the adsorption of phosphorus on $FeCl_3$/LSF. While Freundlich model fitted best to the adsorption of phosphate on LSF.

The value of K_L in Table 3 is related to the affinity of the adsorbent for the solute [45]. As can be seen from Table 3, the K_L value of $FeCl_3$/LSF was higher than that of LSF, indicating that $FeCl_3$/LSF showed higher adsorption capacity towards phosphate than LSF. The adsorption capacity of $FeCl_3$/LSF increased with the increment in temperature, thus higher temperature was favorable for phosphate adsorbing onto $FeCl_3$/LSF and the adsorption of phosphorus on $FeCl_3$/LSF was an endothermic process. Besides, as can been seen from Table 3, the maximum adsorption capacity of phosphate onto $FeCl_3$/LSF calculated from Langmuir model is 13.41 mg g^{-1} at 25°C, which was three times higher than that of LSF. The relatively high adsorption capacity on $FeCl_3$/LSF may due to the strong electrostatic force of attraction between the phosphorus molecules and the binding sites on the

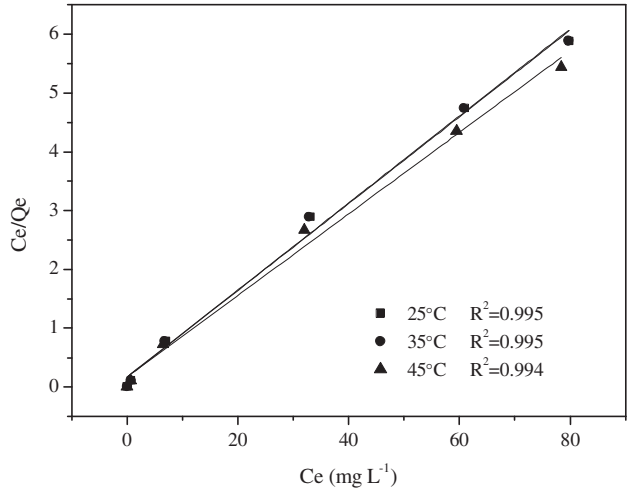

Fig. 9. Langmuir isotherms for phosphate adsorption on $FeCl_3$/LSF.

adsorbent [15]. Besides, larger BET surface area on $FeCl_3$/LSF provides easier access of phosphate. Thus, the adsorption of phosphate onto $FeCl_3$/LSF may involve both physical and chemical adsorption process, which was also confirmed by the SEM–EDS results, FTIR, XRD pattern, and XPS analysis results.

Freundlich isotherm of $FeCl_3$/LSF and LSF are shown in Fig. 10. The calculated value of Freundlich exponent n is a constant related to intensity or energy of adsorption, which represents surface heterogeneity and exponential distribution of active sites and their energies [44]. As can be seen from Table 3, the calculated value of Freundlich exponent n for $FeCl_3$/LSF was 5.73, 5.85, and 5.47 at 25, 35, and 45°C, respectively. A similar value of 5.13 was obtained for phosphorus adsorption onto phosphate mine wastes [15]. These

Table 3
Isotherm parameters for phosphate adsorption on $FeCl_3$/LSF and LSF

Temperature (℃)	Adsorbents	Q_e (mg g^{-1})	Langmuir			Freundlich		
			Q_m (mg g^{-1})	K_L (L mg^{-1})	R^2	n	K_F	R^2
25	$FeCl_3$/LSF	13.39	13.41	0.42	0.995	5.73	6.20	0.999
	LSF	4.59	8.80	0.01	0.711	1.36	0.15	0.985
35	$FeCl_3$/LSF	13.51	13.54	0.43	0.995	5.85	6.36	0.999
	LSF	4.7	9.09	0.01	0.791	1.35	0.16	0.988
45	$FeCl_3$/LSF	14.41	14.43	0.44	0.994	5.47	6.46	0.999
	LSF	4.77	9.13	0.01	0.804	1.35	0.16	0.989

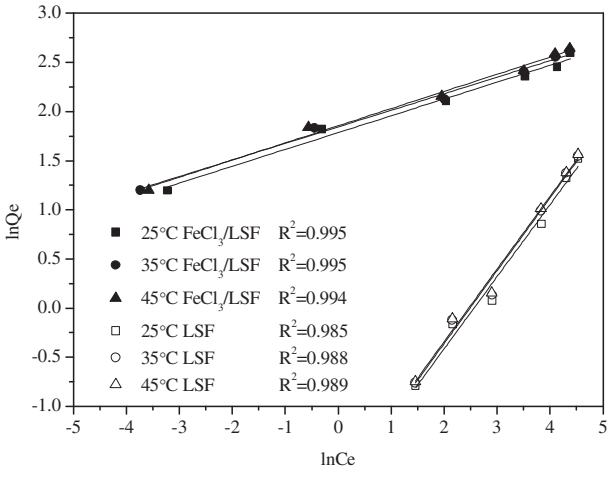

Fig. 10. Freundlich isotherms for phosphate adsorption on $FeCl_3$/LSF and LSF.

values are within the range of 1–10, which indicated a favorable adsorption of phosphate onto $FeCl_3$/LSF [42]. The values of n for $FeCl_3$/LSF were higher than those of LSF. The increase in the value of n for iron oxides modification adsorbents could be attributable to the decrement in the pore diffusion resistance and the change in interactions mechanism between phosphate ions and adsorbent [49].

3.6. Thermodynamic analysis

The influence of temperature on phosphate adsorption was studied at the temperature range of 25–45℃. The thermodynamic equilibrium constants (K_d) of adsorption process were calculated according to the method of Lyubchik et al. [50]. The change in Gibbs free energies (ΔG) was then calculated according to Eq. (9):

$$\Delta G = -RT \ln(K_d) \tag{9}$$

where K_d is the thermodynamic equilibrium constants, R is universal gas constant (8.314 J/mol K), and T is the absolute temperature. The values of free energy were −4.565, −4.77, and −4.80 kJ/mol for $FeCl_3$/LSF, at 25, 35, 45℃, respectively. The negative free energy values indicated the feasibility of the process and the spontaneous nature of adsorption [50]. The values of ΔG decreased from −4.565 to −4.80 kJ mol^{-1} with temperature increasing from 25 to 45℃, indicating the increase in spontaneity at higher temperatures. Besides, more active adsorption sites were available in higher temperature, which would facilitate the phosphate adsorption. This phenomenon is coincident with the results of adsorbing phosphate onto PMS (phosphate mine slimes) and coal fly ash [15,51].

Table 4
Effect of coexisting anions on phosphate removal by $FeCl_3$/LSF

Matrix	Phosphate removal (%)	Adsorption quantity (mg/g)	Initial pH	Final pH
Phosphate	92.6	6.17	6.95	6.87
Phosphate + 0.01 M NaCl	91.3	6.09	6.85	6.76
Phosphate + 0.01 M Na_2SO_4	86.7	5.78	6.88	6.67
Phosphate + 0.01 M $NaNO_3$	90.1	6.0	6.89	6.6
Phosphate + 0.01 M Na_2CO_3	29.8	1.99	10.93	10.53

3.7. Influence of coexisting anion

Some anionic species, such as Cl^-, NO_3^-, SO_4^{2-}, and CO_3^{2-} which may compete with phosphate for adsorption sites, often coexisted in the wastewater and surface water. In order to investigate the practical applicability of $FeCl_3$/LSF, adsorption behavior of $FeCl_3$/LSF in the presence of coexisting anions was studied with 0.01 mol L^{-1} coexisted anions in 0.32 mmol L^{-1} phosphate solutions. Each coexisting anion's concentration was almost 30 times greater than that of phosphate. The result is shown in Table 4, from Table 4, we can find that the presence of 0.01 M Cl^-, NO_3^-, and SO_4^{2-} had slight effect on phosphate adsorption onto $FeCl_3$/LSF. However, the presence of CO_3^{2-} greatly decreased phosphate adsorption capacity, and the removal percentage of phosphate decreased from 92.6 to 29.8% in coexisting system. In the $CO)_3^{2-}$ coexisting system, the initial pH of the phosphate solution was 10.93. Higher pH value would result in more OH^- in the solution, which would compete with the adsorption sites on phosphate. What's more, the surface of $FeCl_3$/LSF was negatively charged at higher pH values (pH_{ZPC} = 5.45), which would cause electrostatic repulsion between the phosphate and the $FeCl_3$/LSF, thus reducing the adsorption of phosphate.

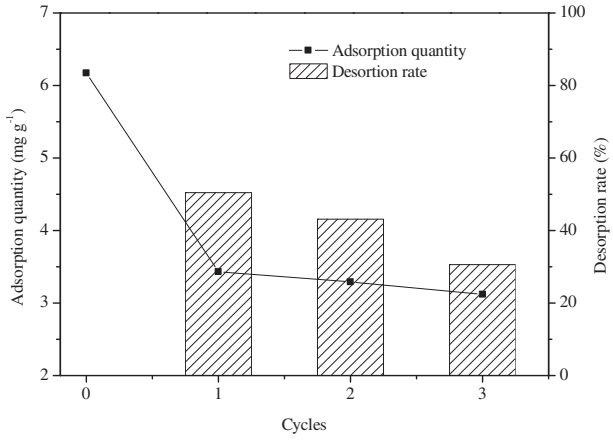

Fig. 11. Regeneration of $FeCl_3$/LSF.

3.8. Regeneration of $FeCl_3$/LSF

The adsorption capacity of phosphate by original and regenerated $FeCl_3$/LSF, as well as it's desorption rate are shown in Fig. 11. As can be seen from Fig. 11, the adsorption capacity of $FeCl_3$/LSF decreased from 6.17 to 3.43 mg g^{-1} after its first regeneration cycle, and the adsorption capacity was maintained at around 3 mg g^{-1} for the next two cycles. A relatively low desorption rate was observed from the desorption result, with the value between 30 and 50%. This may due to the formation of chemical complexes during adsorption, which can hardly be desorbed. This assumption is consistent with XRD analysis, which showed the formation of $Fe(PO_3)_3$ complex on the surface of $FeCl_3$/LSF after adsorbing phosphate. In other words, phosphate adsorption on the surface of $FeCl_3$/LSF may involve chemisorption.

3.9. Comparison of phosphate adsorption ability

Table 5 shows the comparison of the maximum phosphate adsorption capacity obtained in the present study with other iron-containing adsorbents from previous study. It can be seen that the phosphate adsorption capacity of $FeCl_3$/LSF was relatively high compared with the other adsorbents. Besides, less than 0.1 mg L^{-1} Fe^{3+} was detected in the solution from the

Table 5
Comparison of phosphate adsorption capacities (Q_m) for various adsorbents

Material	Q_m (mg g^{-1})	Refs.
Ferric sludge	25.5	[19]
Red mud	0.8	[17]
Iron oxide tailing	8.21	[37]
Iron-coated sand	0.322	[36]
Innovative modified bentonites (Zenith/Fe)	11.15	[52]
Goethite	6.42	[53]
Ferric oxides loading biochar	0.963	[54]
Iron-doped activated carbon	14.1	[8]
Iron hydroxide-eggshell	2.02	[7]
Synthetic iron oxide coated sand	1.5	[34]
$FeCl_3$/LSF (298 K)	13.39	Present study

leaching study of $FeCl_3$/LSF. Therefore, $FeCl_3$/LSF is a potential attractive adsorbent to remove phosphate from aqueous solution.

4. Conclusions

The present study demonstrated that $FeCl_3$/LSF could be used as an effective adsorbent for phosphate removal from aqueous solution. The experimental results showed that $FeCl_3$/LSF, $Fe(NO_3)_3$/LSF and $Fe_2(SO_4)_3$/LSF exhibited higher phosphate removal capacity than unmodified LSF, indicating that iron oxides modification could improve the phosphate removal capacity of LSF. Among three iron oxide modified LSF, $FeCl_3$/LSF exhibited the highest adsorption capacity, with maximum adsorption capacity of 13.39 mg g^{-1} at 25°C. The kinetic studies showed that the adsorption of $FeCl_3$/LSF agreed well with the pseudo-second-order. Coexisting ions experiment results showed that Cl^-, NO_3^-, and SO_4^{2-} had slight influence on phosphate removal, while CO_3^{2-} significantly reduced the adsorption of phosphate. From the results of desorption study, together with characterization analysis from SEM-EDS, FTIR, XRD, and XPS, we can conclude that the adsorption of phosphate by $FeCl_3$/LSF involves both physisorption and chemisorption process. The high adsorption capacity of $FeCl_3$/LSF demonstrates it is an efficient adsorbent for removal of phosphate from wastewater at low cost.

Acknowledgments

The authors are grateful for the help from Project 2015SCU11028.

References

[1] D. Cordell, J.-O. Drangert, S. White, The story of phosphorus: Global food security and food for thought, Global Environ. Change 19 (2009) 292–305.
[2] N.C. Woods, S.M. Sock, G.T. Daigger, Phosphorus recovery technology modeling and feasibility evaluation for municipal wastewater treatment plants, Environ. Technol. 20 (1999) 663–679.
[3] J. Xie, Z. Wang, S. Lu, D. Wu, Z. Zhang, H. Kong, Removal and recovery of phosphate from water by lanthanum hydroxide materials, Chem. Eng. J. 254 (2014) 163–170.
[4] S.A. Parsons, J.A. Smith, Phosphorus removal and recovery from municipal wastewaters, Elements 4 (2008) 109–112.
[5] G.M. Filippelli, The global phosphorus cycle: Past, present, and future, Elements 4 (2008) 89–95.
[6] J. Xie, Z. Wang, D. Wu, Z. Zhang, H. Kong, Synthesis of zeolite/aluminum oxide hydrate from coal fly ash: A new type of adsorbent for simultaneous removal of cationic and anionic pollutants, Ind. Eng. Chem. Res. 52 (2013) 14890–14897.
[7] N.Y. Mezenner, A. Bensmaili, Kinetics and thermodynamic study of phosphate adsorption on iron hydroxide-eggshell waste, Chem. Eng. J. 147 (2009) 87–96.
[8] Z. Wang, E. Nie, J. Li, M. Yang, Y. Zhao, X. Luo, Z. Zheng, Equilibrium and kinetics of adsorption of phosphate onto iron-doped activated carbon, Environ. Sci. Pollut. Res. 19 (2011) 2908–2917.
[9] A. Ugurlu, B. Salman, Phosphorus removal by fly ash, Environ. Int. 24 (1998) 911–918.
[10] J. Yang, L. Zhou, L. Zhao, H. Zhang, J. Yin, G. Wei, K. Qian, Y. Wang, C. Yu, A designed nanoporous material for phosphate removal with high efficiency, J. Mater. Chem. 21 (2011) 2489–2494.
[11] W. Chouyyok, R.J. Wiacek, K. Pattamakomsan, T. Sangvanich, R.M. Grudzien, G.E. Fryxell, W. Yantasee, Phosphate removal by anion binding on functionalized nanoporous sorbents, Environ. Sci. Technol. 44 (2010) 3073–3078.
[12] L.E. de-Bashan, Y. Bashan, Recent advances in removing phosphorus from wastewater and its future use as fertilizer (1997–2003), Water Res. 38 (2004) 4222–4246.
[13] P. Pengthamkeerati, T. Satapanajaru, P. Chularuengoaksorn, Chemical modification of coal fly ash for the removal of phosphate from aqueous solution, Fuel 87 (2008) 2469–2476.
[14] J. Chen, H. Kong, D. Wu, X. Chen, D. Zhang, Z. Sun, Phosphate immobilization from aqueous solution by fly ashes in relation to their composition, J. Hazard. Mater. 139 (2007) 293–300.
[15] S. Jellali, M.A. Wahab, R. Ben Hassine, A.H. Hamzaoui, L. Bousselmi, Adsorption characteristics of phosphorus from aqueous solutions onto phosphate mine wastes, Chem. Eng. J. 169 (2011) 157–165.
[16] G. Akay, B. Keskinler, A. Çakici, U. Danis, Phosphate removal from water by red mud using crossflow microfiltration, Water Res. 32 (1998) 717–726.
[17] W. Huang, S. Wang, Z. Zhu, L. Li, X. Yao, V. Rudolph, F. Haghseresht, Phosphate removal from wastewater using red mud, J. Hazard. Mater. 158 (2008) 35–42.
[18] Y. Li, C. Liu, Z. Luan, X. Peng, C. Zhu, Z. Chen, Z. Zhang, J. Fan, Z. Jia, Phosphate removal from aqueous solutions using raw and activated red mud and fly ash, J. Hazard. Mater. 137 (2006) 374–383.
[19] X. Song, Y. Pan, Q. Wu, Z. Cheng, W. Ma, Phosphate removal from aqueous solutions by adsorption using ferric sludge, Desalination 280 (2011) 384–390.
[20] Y. Yang, Y.Q. Zhao, A.Q. Babatunde, L. Wang, Y.X. Ren, Y. Han, Characteristics and mechanisms of phosphate adsorption on dewatered alum sludge, Sep. Purif. Technol. 51 (2006) 193–200.
[21] W. Huang, Y. Zhu, J. Tang, X. Yu, X. Wang, D. Li, Y. Zhang, Lanthanum-doped ordered mesoporous hollow silica spheres as novel adsorbents for efficient phosphate removal, J. Mater. Chem. A 2 (2014) 8839–8848.
[22] W. Zhang, Y. Tian, Phosphorous removal from wastewater by lanthanum modified Y zeolites, Front. Chem. Sci. Eng. 9 (2015) 209–215.
[23] H. Nadaroglu, A.A. Gungor, N. Celebi, Removal of Basic Red 9 (BR9) in aqueous solution by using silica with nano-magnetite by enzymatic with Fenton process, Int. J. Environ. Res. 9 (2015) 991–1000.

[24] H. Nadaroglu, N. Celebi, E. Kalkan, N. Dikbas, The Evaluation of Affection of Methylobacterium extorquens—Modified silica fume for adsorption cadmium (II) ions from aqueous solutions affection, Kafkas Univ. Vet. Fak. 19 (2013) 391–397.
[25] H. Nadaroglu, E. Kalkan, Removal of copper from aqueous solution using activated silica fume with/without apocarbonic anhydrase, Indian. J. Chem. Technol. 21 (2014) 249–256.
[26] E. Kalkan, H. Nadaroglu, N. Demir, Experimental study on the nickel (II) removal from aqueous solutions using silica fume with/without apocarbonic anhydrase, Desalin. Water Treat. 44 (2012) 180–189.
[27] E. Kalkan, H. Nadaroğlu, N. Celebi, G. Tozsin, Removal of textile dye Reactive Black 5 from aqueous solution by adsorption on laccase-modified silica fume, Desalin. Water Treat. 52 (2014) 6122–6134.
[28] E. Kalkan, H. Nadaroglu, N. Celebi, Use of silica fume as low-cost absorbent material for nickel removal from aqueous solutions, Asian J. Chem. 26 (2014) 6121–6126.
[29] K. Reitzel, F.Ø. Andersen, S. Egemose, H.S. Jensen, Phosphate adsorption by lanthanum modified bentonite clay in fresh and brackish water, Water Res. 47 (2013) 2787–2796.
[30] E.W. Shin, K.G. Karthikeyan, M.A. Tshabalala, Orthophosphate sorption onto lanthanum-treated lignocellulosic sorbents, Environ. Sci. Technol. 39 (2005) 6273–6279.
[31] M. Zamparas, G. Gavriil, F.A. Coutelieris, I. Zacharias, A theoretical and experimental study on the P-adsorption capacity of Phoslock™, Appl. Surf. Sci. 335 (2015) 147–152.
[32] M.J. Barry, B.J. Meehan, The acute and chronic toxicity of lanthanum to Daphnia carinata, Chemosphere 41 (2000) 1669–1674.
[33] X. Wang, Z. Liu, J. Liu, M. Huo, H. Huo, W. Yang, Removing phosphorus from aqueous solutions using lanthanum modified pine needles, Plos One 10 (2015) e0142700.
[34] N. Boujelben, J. Bouzid, Z. Elouear, M. Feki, F. Jamoussi, A. Montiel, Phosphorus removal from aqueous solution using iron coated natural and engineered sorbents, J. Hazard. Mater. 151 (2008) 103–110.
[35] Q. Zhou, J. Liu, G. Qian, J. Zhou, Granular laterite for batch and column studies of phosphate removal and its modification with iron for enhancing the adsorption property, Desalin. Water Treat. 54 (2015) 1204–1215.
[36] Y.X. Huang, J.K. Yang, A.A. Keller, Removal of arsenic and phosphate from aqueous solution by metal (hydr-)oxide coated sand, ACS Sustainable Chem. Eng. 2 (2014) 1128–1138.
[37] L. Zeng, X.M. Li, J.D. Liu, Adsorptive removal of phosphate from aqueous solutions using iron oxide tailings, Water Res. 38 (2004) 1318–1326.
[38] E.J. Elzinga, R. Kretzschmar, In situ ATR-FTIR spectroscopic analysis of the co-adsorption of orthophosphate and Cd(II) onto hematite, Geochim. Cosmochim. Acta 117 (2013) 53–64.
[39] M. Jang, S.H. Min, T.H. Kim, J.K. Park, Removal of arsenite and arsenate using hydrous ferric oxide incorporated into naturally occurring porous diatomite, Environ. Sci. Technol. 40 (2006) 1636–1643.
[40] T.A. Ngantcha, R. Vaughan, B.E. Reed, Modeling As (III) and As(V) removal by an iron oxide impregnated activated carbon in a binary adsorbate system, Sep. Purif. Technol. 46 (2011) 1419–1429.
[41] R.C. Vaishya, S.K. Gupta, Arsenic removal from groundwater by iron impregnated sand, J. Environ. Eng. 129 (2003) 89–92.
[42] J. Su, H.-G. Huang, X.-Y. Jin, X.-Q. Lu, Z.-L. Chen, Synthesis, characterization and kinetic of a surfactant-modified bentonite used to remove As(III) and As(V) from aqueous solution, J. Hazard. Mater. 185 (2011) 63–70.
[43] Z. Wen, Y. Zhang, C. Dai, Removal of phosphate from aqueous solution using nanoscale zerovalent iron (nZVI), Colloids Surf. A 457 (2014) 433–440.
[44] P.R. Rout, P. Bhunia, R.R. Dash, A mechanistic approach to evaluate the effectiveness of red soil as a natural adsorbent for phosphate removal from wastewater, Desalin. Water Treat. 54 (2015) 358–373.
[45] L.-G. Yan, K. Yang, R.-R. Shan, T. Yan, J. Wei, S.-J. Yu, H.-Q. Yu, B. Du, Kinetic, isotherm and thermodynamic investigations of phosphate adsorption onto core-shell Fe_3O_4@LDHs composites with easy magnetic separation assistance, J. Colloid Interface Sci. 448 (2015) 508–516.
[46] N.I. Chubar, V.A. Kanibolotskyy, V.V. Strelko, G.G. Gallios, V.F. Samanidou, T.O. Shaposhnikova, V.G. Milgrandt, I.Z. Zhuravlev, Adsorption of phosphate ions on novel inorganic ion exchangers, Colloids Surf. A 255 (2005) 55–63.
[47] J.T.N. Knijnenburg, E. Seristatidou, F.M. Hilty, F. Krumeich, Y. Deligiannakis, Proton-promoted iron dissolution from nanoparticles and the influence by the local iron environment, J. Phys. Chem. C 118 (2014) 24072–24080.
[48] A. Olgun, N. Atar, S. Wang, Batch and column studies of phosphate and nitrate adsorption on waste solids containing boron impurity, Chem. Eng. J. 222 (2013) 108–119.
[49] S. Karaca, A. Gurses, M. Ejder, M. Acikyildiz, Adsorptive removal of phosphate from aqueous solutions using raw and calcinated dolomite, J. Hazard. Mater. 128 (2006) 273–279.
[50] S.I. Lyubchik, A.I. Lyubchik, O.L. Galushko, L.P. Tikhonova, J. Vital, I.M. Fonseca, S.B. Lyubchik, Kinetics and thermodynamics of the Cr(III) adsorption on the activated carbon from co-mingled wastes, Colloids Surf. A 242 (2004) 151–158.
[51] S.S. Choi, J.C. Chung, S.H. Yeom, Removal of phosphate using coal fly ash from a thermal power station, J. Ind. Eng. Chem. 11 (2005) 638–642.
[52] M. Zamparas, A. Gianni, P. Stathi, Y. Deligiannakis, I. Zacharias, Removal of phosphate from natural waters using innovative modified bentonites, Appl. Clay Sci. 62–63 (2012) 101–106.
[53] O.K. Borggaard, B. Raben-Lange, A.L. Gimsing, B.W. Strobel, Influence of humic substances on phosphate adsorption by aluminium and iron oxides, Geoderma 127 (2005) 270–279.
[54] J. Ren, N. Li, L. Li, J.-K. An, L. Zhao, N.-Q. Ren, Granulation and ferric oxides loading enable biochar derived from cotton stalk to remove phosphate from water, Bioresour. Technol. 178 (2015) 119–125.